Water Dispersible Carbohydrate-Coated Ferrite Nanoparticles. Effect of Cobalt Doping in Magneto-Thermal Properties

Lenaic Lartigue, Claudia Innocenti, Joulia Larionova, Yannick Guari

Article

Journal of
Nanoscience and Nanotechnology
Vol. 19, 1–8, 2019
www.aspbs.com/jnn

Water Dispersible Carbohydrate-Coated Ferrite Nanoparticles. Effect of Cobalt Doping in Magneto-Thermal Properties

Lenaic Lartigue[1, 2, *], Claudia Innocenti[3, 4], Joulia Larionova[1], and Yannick Guari[1]

[1] *ICGM, Univ. Montpellier-CNRS-ENSCM, Place E. Bataillon, Montpellier, France*
[2] *CEISAM–UMR CNRS 6230, Université de Nantes, 2 rue de la Houssinière, 44322 Nantes, France*
[3] *ICCOM-CNR via Madonna del Piano 10, 50019 Sesto Fiorentino, Italy*
[4] *INSTM and Dipartimento di Chimica "U. Schiff", Università degli Studi di Firenze, via della Lastruccia 3, I-50019 Sesto Fiorentino, Italy*

Water dispersible cobalt ferrite nanoparticles, $Co_xFe_{3-x}O_4$, of different size (4–10 nm) and various composition ($0 \leq x \leq 1$), functionalized with a rhamnose derivative were obtained and characterized by combining TEM, XRD and elemental analyses techniques. Magnetic properties of these systems were studied by SQUID magnetometry. A particular emphasis was given to the investigation of magnetocrystalline anisotropy and size effect on the heating abilities of the nanoparticles under the application of an alternating magnetic field.

Keywords: Cobalt Ferrite, Magnetic Hyperthermia, Water Soluble NPs, Magnetocrystalline Anisotropy.

1. INTRODUCTION

Due to their biocompatibility, iron oxide nanoparticles like maghemite (γ-Fe_2O_3) and magnetite (Fe_3O_4) have widely been developed for biomedical applications.[1] Mixed ferrites with general formula $M_xFe_{3-x}O_4$, obtained by substituting Fe^{2+} with other metal ions (M^{2+}, where M = Co, Mn, Ni, Zn...), has been often suggested for tuning the magnetic properties. Among different bivalent transition metal ions, the use of Co^{2+} to form cobalt ferrite nanoparticles is very promising because it induces an important increase of the magneto-crystalline anisotropy, which provides a significant improvement of the magneto-thermal properties of particles of a few nanometers (<20 nm), allowing their effective use as heat-mediator for magnetic fluid hyperthermia.[2] In order to design cobalt ferrite nanoparticles for biomedical application and, in particular, for hyperthermia treatment, different requirements must be addressed, such as stability at physiological pH, good dispersibility in water, biocompatibility, non-toxicity for living organisms, non-interaction with immune cells, efficiency for the specific application, etc.[3–5] In addition to the chemical composition, the efficiency of nanoparticles as mediator for magnetic hyperthermia depends on their size and the size distribution.[6] The synthesis of water dispersible cobalt ferrite nanoparticles with a precise size and composition control is a challenge because the classical co-precipitation or microemulsion methods in aqueous media leads to nanoparticles with a relatively large size distribution.[7–11] To fix this problem, polyol approaches have been developed for small size nanoparticles,[12] however, the size and shape distribution is commonly very limited.[13–16] By contrast, thermal decomposition is a more versatile approach giving very homogenous but hydrophobic nanoparticles.[17] Up to date, only a few publications report on the synthesis of water dispersible cobalt ferrite nanoparticles.[18] We have already reported[19] a two-step approach to the synthesis of carbohydrates-coated magnetite nanoparticles with sizes in the range 4–35 nm. In this approach, nanoparticles with a narrow size distribution were prepared by a thermal decomposition method followed by a ligand exchange with carbohydrate ligand in order to achieve a good water dispersibility. The surface functionalization of nanoparticles with carbohydrates presents several advantages like (i) water dispersibility and biocompatibility and (ii) cellular recognition thanks to carbohydrate-binding proteins.[20, 21] In particular, rhamnose moieties have demonstrated a specificity on the recognition of skin cells of the epidermis or the horny

*Author to whom correspondence should be addressed.

layer.[22] In this work, we present the synthesis of water-dispersible cobalt ferrite nanoparticles having different size and composition and functionalized by a rhamnose derivative. The relationships between nanoparticles size, composition and magnetic and magneto-thermal properties are investigated.

2. EXPERIMENTAL DETAILS

2.1. Reagents

Absolute ethanol, hexane, methanol and dichloromethane (99%) were used as received. The THF was purified by distillation over sodium. 1,2-hexadecanediol (90%), oleic acid (90%), ammonia 2.0 M solution in methanol, cobalt(II) acetylacetonate (97%), tris(trimethylsilyl)phosphate (≥98%), triethylene glycol (Reagent Plus, 99%), boron trifluoride etherate (≥46% BF_3 basis), tetrabromomethane (Reagent Plus, 99%), triphenylphosphite (97%) were purchased from Aldrich Chemical Co. Phenyl ether (99%), Benzyl ether (98%), oleylamine approximate C18 content 80–90% (97%), iron(III) acetylacetonate (99+%), were purchased from Acros Organics. Rhamnose was purchased from Benn Chemicals.

2.2. Preparation of Cobalt Ferrite Nanoparticles

Non stoichiometric cobalt ferrite nanoparticles were synthesized by adopting the experimental conditions of the procedure previously reported by Sun et al.[17] Samples of different size, *d*, and cobalt content, *x*, were obtained by changing the experimental parameters. The final products were denoted as **Co_xFe-d**. As a typical example, to obtain **$Co_{0.5}$Fe-4** nanoparticles, $Fe(acac)_3$ (2 mmol), $Co(acac)_2$ (1 mmol), 1,2-hexadecanediol (10 mmol), oleic acid (6 mmol), oleylamine (6 mmol), and phenyl ether (20 mL) were mixed and magnetically stirred under a flow of argon. Nanoparticles were obtained in inert atmosphere by a two-step heating procedure, first at 200 °C for 30 min and then, at reflux (at 265 °C) for 30 min. Once the solution was cooled down to the ambient temperature, 40 mL of ethanol was added to precipitate the nanoparticles, which were separated by centrifugation (15000 rpm, 10 min). Then, the supernatant was removed and the powder dispersed in hexane. Another centrifugation (5000 rpm, 5 min) was performed to remove any undispersed residue. Finally, a last washing was realized by adding ethanol and making centrifugation (15000 rpm, 10 min). The synthesis permits to obtain 170 mg of a black powder soluble in hexane (yield: 25%). **$Co_{0.4}$Fe-6** and **$Co_{0.3}$Fe-6** were obtained with the same procedure and in the same yield but using 20 mL and 10 mL of benzyl ether, respectively.

Stoichiometric cobalt ferrite nanoparticles (**Co_1Fe-4, Co_1Fe-6, Co_1Fe-10**) were obtained by adapting the procedure proposed by Hou et al. for the wüstite nanoparticles.[23] To prepare **Co_1Fe-10** nanoparticles, 1.4 g of $Fe(acac)_3$ (4 mmol) and 0.6 g of $Co(acac)_2$ (2.30 mmol) were mixed with oleic acid (10 mL) and oleylamine (10 mL), then a preliminary heating step of 2 hours at 100 °C under a partial vacuum was applied. Under argon atmosphere, two heating steps at 200 °C for 30 min and the second at 280 °C for 30 min were done. **Co_1Fe-4** nanoparticles were obtained by mixing 8 mL of oleic acid and 12 mL of oleylamine. With the same procedure as **Co_1Fe-4**, the **Co_1Fe-6** nanoparticles were obtained by increasing the preliminary heating step from 100 °C to 130 °C. The washing procedure was the same as described previously. The synthesis of magnetite reference samples, **Co_0Fe-4**, **Co_0Fe-6** nanoparticles was performed as previously described.[19]

2.3. Functionalization of Cobalt Ferrite Nanoparticles

The functionalization of nanoparticles by a rhamnose derivative was operated in two steps as previously described for magnetite nanoparticles.[19,24] Briefly, 0.46 mmol of oleic acid/oleylamine-coated iron-based oxide nanoparticles and 0.78 mmol of rhamnose were dissolved in anhydrous THF (5 mL). The mixture was magnetically stirred under argon to reflux for 48 h. Under standard conditions, pentane (30 mL) was added to the mixture, and the solid was precipitated and separated via centrifugation. The product was dissolved in hexane and the undispersed residue was removed by centrifugation (120000 rpm, 10 min). The solution was then precipitated with ethanol (40 mL) and separated via centrifugation. Then, 0.2 mmol of the nanoparticles obtained in the first step was dissolved in a solution of ammonia methanol 2 M (10 mL). The solution was magnetically stirred under argon at ambient condition for 4 h. Dichloromethane (30 mL) was then added to the mixture, and the solid was precipitated and separated via centrifugation. The washing procedure consisted in resuspension of the solid product in hexane and its precipitation in ethanol. Then, a centrifugation cycle (120000 rpm, 10 min) was applied twice.

2.4. Characterizations

Samples for Transmission Electronic Microscopy (TEM) measurements were prepared by depositing a drop of an ethanol solution of the nanoparticles on the carbon coated copper grids. The measurements were carried out with a microscope JEOL 1200 EXII operated at 100 kV. The size of the nanoparticles was statistically determined over a large number of units (200–300) using SigmaPro Scan software which provides the mean diameter and the polydispersity of the ensemble. The average hydrodynamic diameter, d_H, and its dispersion were determined by Dynamic Light Scattering (DLS) performed by Malvern High Performance Particle Sizer operating at 635 nm. The decay of the correlation function was fitted by a cumulant function. IR spectra were recorded by using a Perkin Elmer 1600 spectrometer with a 4 cm^{-1} resolution. Samples were prepared as pellets in a KBr matrix. KBr was stored in oven and pellets pressed under vacuum to minimize water traces. Elemental analyses were performed by

the Service Central d'Analyse (CNRS, Vernaison, France). The samples were heated at 3000 °C under He, the oxygen was transformed in CO and detected by using an IR detector. An evaluation of the Fe/P ratio was also performed by using an Environmental Secondary Electron Microscope FEI Quanta 200 FEG coupled with an Electrons Dispersive Spectroscope Oxford INCA detector. Powder X-ray diffraction patterns were measured at room temperature on a PanAnalytical diffractometer equipped with an ultra-fast X'celerator detector X'pert Pro with Nickel-filtered copper radiation (1.5405 Å) and on a Bruker D8 Advance diffractometer equipped with Cu Kα radiation and operating in θ–2θ Bragg Brentano geometry at 40 kV and 40 mA. Magnetic measurements were collected with a Quantum Design MPMS-XL SQUID magnetometer working in the temperature range of 1.8–300 K and in the magnetic field range of 0–50 kOe. Zero Field Cooled (ZFC)/Field Cooled (FC) magnetizations were acquired with a 5 mT probe field after cooling the sample with (FC) and without (ZFC) the field applied.

2.5. Evaluation of Magnetothermal Properties

The evaluation of the heat generation capability was performed with an in-house built magnetothermal setup based on a Nova Star 5 kW® (Ameritherm Inc.) generator. A solution of rhamnose-coated magnetic nanoparticles was put in a thermic insulating support inside the induction coil and the temperature was measured with a VR18_CR® digital temperature recorder (Ceam Group) connected to an optical fiber directly dipped into the sample. The study was performed with 300 μL of a 20 mM suspension of nanoparticles. Frequency and amplitude of the applied alternating magnetic were $f = 168$ kHz and $H = 21$ kA/m. Heating capability was estimated by the Specific Absorption Rate (SAR) evaluated from the initial slope (dT/dt) of the measured kinetic temperature curve, $T(t)$, by using the following formula:

$$\mathrm{SAR} = \frac{1}{m_{\mathrm{CoFe}}}\left(\sum_i c_i m_i \frac{dT}{dt}\right)$$

where m_{CoFe} is the total mass of the metal, c_i is the specific heat and m_i the mass of the i-th species in the solution.

3. RESULTS AND DISCUSSION

3.1. Synthesis of Rhamnose Functionalized Cobalt Ferrites Nanoparticles

The synthesis of the rhamnose-functionalized $Co_xFe_{3-x}O_4$ (with $0 \leq x \leq 1$) nanoparticles was performed using a three-steps approach shown in Figure 1, we previously used for the synthesis of magnetite nanoparticles.[19, 24] The first step consists in the synthesis of oleic acid/oleyl amine coated $Co_xFe_{3-x}O_4$ nanoparticles using the well-known flash decomposition synthesis giving nanoparticles with a narrow size distribution and high crystallinity. Note that non-stoichiometric cobalt ferrite nanoparticles were obtained with phenyl or benzylether as solvent, 1-2 hexadecanediol as the reducing agent and the oleic acid/oleylamine mixture as stabilizing agents, while stoichiometric cobalt ferrite nanoparticles were obtained when the oleic acid/oleylamine mixture was used both as the stabilizing agent and the solvent. The as-obtained nanoparticles are well dispersible in hexane. To transfer these nanoparticles in water, a ligand exchange was performed in the second step by using a rhamnose derivative with a phosphonate anchoring function. The rhamnose derivative functionalized with a phosphonate coordinative moiety replaces the oleic acid/oleyl amine at the nanoparticles' surface with a covalent anchoring. The third step is the deprotection of the rhamnose part of the ligand in the mixture $MeOH/NH_3$ to obtain rhamnose-functionalized nanoparticles, denoted as **Rha{Co_xFe-Size}** (Table I) where x is the content of Co.

The effectiveness of the ligand exchange is confirmed by the final solubility of the nanoparticles in water and is verified by Fourier-transform Infrared Spectroscopy. After functionalization, an appearance of the characteristic vibration bands of the carbohydrate derivative was observed, i.e., the broad band centered at 1050 cm^{-1}, which is attributed to the ν(P–O–Fe), ν(COC) and

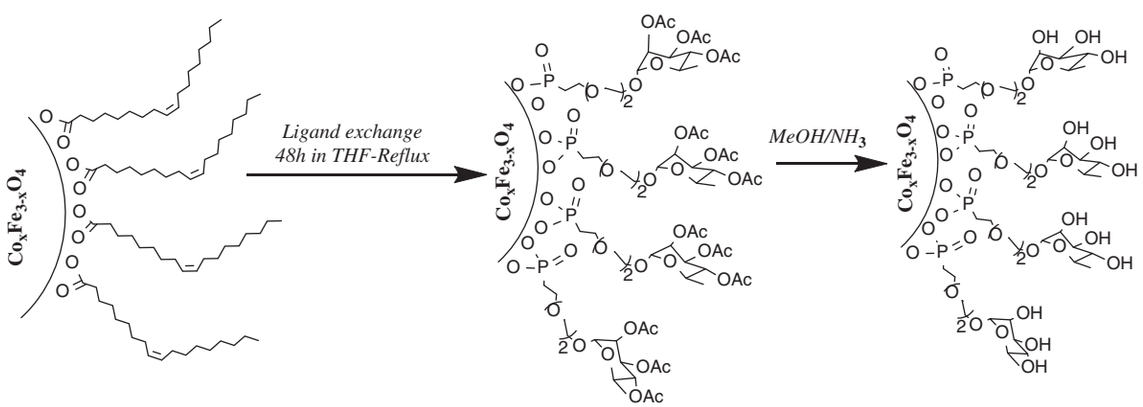

Figure 1. Schematic representation of the synthesis of rhamnose-functionalized $Co_xFe_{3-x}O_4$ nanoparticles.

Table I. Structural characterization and magnetic properties in DC mode of $Co_xFe_{3-x}O_4$ nanoparticles. x, cobalt content obtained from elemental analysis; $\langle d_{TEM}\rangle$, mean particle size and σ, polydispersity statistically obtained from TEM images; $\langle d_{XRD}\rangle$, mean particle size from XRD pattern by using Debye-Sherrer formula on the (311) diffraction peak (the accuracy of the fitting parameter estimation induces errors on $\langle d_{XRD}\rangle$ largely within 10% for all the samples); d_H, hydrodynamic diameter obtained by DLS. $T_{max} \sim T_B$, maximal temperature of the ZFC curve, identified with the blocking temperature, T_B, of the systems. M_R/M_S, reduced remnant magnetization; $\mu_0 H_C$, coercive field; M_S, saturation magnetization at 2.5 K; K, anisotropy constant, obtained from the hysteresis loop at 2.5 K; and SAR, specific absorption rate. Errors on M_S value are principally due to cobalt and iron assay (precision of 5%), the accuracy on the magnetic quantities indirectly evaluated (T_{max}, H_c and K) can be estimated within 1%. The accuracy of the SAR values can be roughly estimated from the initial slope linear fit and iron and cobalt assay quality as large as 10 % for low value and 5% for high value.

					M (T)	M (H) at 2.5 K				
	x	$\langle d_{TEM}\rangle$ (σ)/nm	$\langle d_{XRD}\rangle$ (error)/nm	d_H (error)/nm	T_{max} (error)/K	M_R/M_S (error)	$\mu_0 H_C$ (error)/T	M_S (error)/ $A\cdot m^2\cdot kg^{-1}$	$K\times 10^5$ (error)/$J\cdot m^{-3}$	SAR (error)/W/g
Rha{Co_0Fe-4}	0.00	4.1 (0.15)	4.5 (0.5)	8.2 (1.3)	17 (1)	0.26 (0.01)	0.036 (0.001)	96 (5)	0.24 (0.01)	0 (1)
Rha{$Co_{0.5}$Fe-4}	0.53	4.5 (0.20)	4.7 (0.5)	10.0 (2.7)	183 (2)	0.73 (0.01)	1.48 (0.02)	67 (4)	5.6 (0.1)	6 (1)
Rha{Co_1Fe-4}	1.00	4.8 (0.17)	4.5 (0.5)	10.2 (1.8)	213 (2)	0.83 (0.01)	1.53 (0.02)	56 (3)	4.9 (0.01)	21 (3)
Rha{Co_0Fe-6}	0.00	6.7 (0.12)	6.7 (0.7)	10.4 (1.5)	58 (1)	0.37 (0.01)	0.041 (0.001)	94 (5)	0.23 (0.01)	2 (1)
Rha{$Co_{0.3}$Fe-6}	0.31	7.5 (0.17)	7.2 (0.7)	14.1 (2.7)	260 (3)	0.91 (0.01)	1.81 (0.02)	78 (4)	8.0 (0.1)	44 (5)
Rha{$Co_{0.4}$Fe-6}	0.38	6.8 (0.22)	7.1 (0.7)	13.2 (3.3)	314 (4)	0.83 (0.01)	2.08 (0.03)	81 (5)	9.5 (0.1)	22 (3)
Rha{Co_1Fe-6}	1.00	5.8 (0.21)	5.5 (0.6)	12.5 (2.1)	259 (3)	0.82 (0.01)	1.61 (0.02)	79 (4)	7.3 (0.1)	32 (4)
Rha{Co_1Fe-10}	1.00	9.7 (0.22)	10 (1)	18.1 (5.4)	/	0.86 (0.01)	1.86 (0.02)	76 (4)	8.0 (0.1)	232 (12)

$\nu(CH_{cycle})$ elongations. The characteristic broad band at 570 cm^{-1}, attributed to ν(Fe–O) bands of $Co_xFe_{3-x}O_4$, was preserved during the three steps indicating that the structure of $Co_xFe_{3-x}O_4$ after the carbohydrate anchorage and deprotection remained unchanged.

TEM images of the obtained nanoparticles are shown in Figure 2. The average diameter, $\langle d_{TEM}\rangle$, and the standard deviation, σ, of the magnetic cores are summarized in Table I. Each sample shows nanoparticles with a spherical-like shape and σ less than 22%.

The powder X-ray diffraction patterns (XRD) within the range of $2\theta = 20$–$70°$ are shown in Figure 3. All diffractograms exhibit diffraction peaks indexed as (220), (311), (400), (422), (511) and (440) reflections, characteristic of the spinel structure of ferrite. The mean diameter of crystalline domains, $\langle d_{XRD}\rangle$, estimated by the Debye-Scherrer formula and reported in Table I, is in good agreement with d_{TEM}, evidencing the high crystallinity of all the samples. The hydrodynamic diameters of the nanoparticles, d_H, determined by DLS are larger than d_{TEM}, as expected, but less than or similar to 2 d_{TEM} for most of the samples proving the good dispersion (no magnetic core aggregation) of nanoparticles in water. The cobalt content (x) was obtained by elemental analysis and indicated in Table I.

3.2. Magnetic Properties

Temperature dependence of the ZFC/FC magnetization curves measured in solution are presented in Figures 4(A) and (C) for the nanoparticles with size of 4 nm and

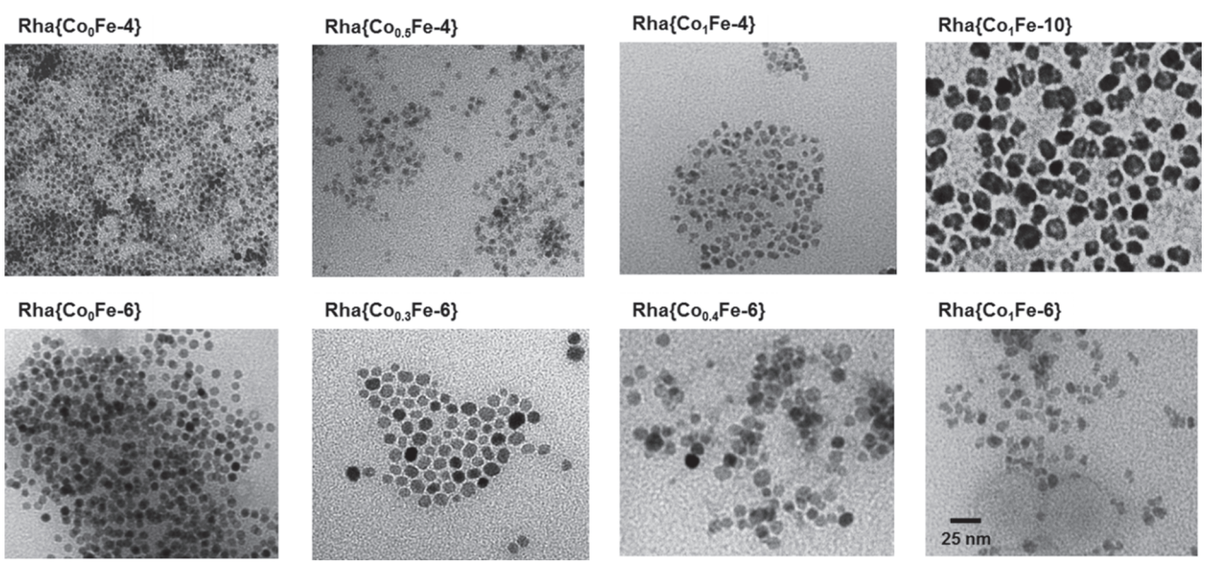

Figure 2. Representative TEM micrographs of $Co_xFe_{3-x}O_4$ nanoparticles. The scale bar, reported in the last image, is the same over the series.

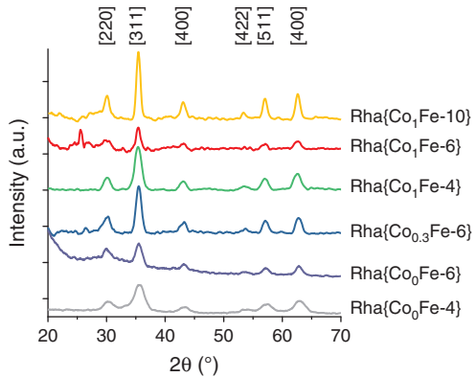

Figure 3. X-ray diffraction patterns within the range of 2θ (20–70°) of $Co_xFe_{3-x}O_4$ nanoparticles. The higher background of Rha{$Co_{0.3}$Fe-6} is due to a larger amount of organic coating present in the sample.

6-nm, respectively. In both series, a significant increase of T_{max}, the temperature at which the ZFC curve achieves its maximum, is observed for samples doped with Co^{2+} in comparison with magnetite nanoparticles of the same size, and, except for **Rha{Co_1Fe-6}**, it increases upon Co content. Moreover, for stoichiometric cobalt ferrite samples, T_{max} value raises with increasing size. Both trends are expected since T_{max} is commonly associate with the blocking temperature, T_B, of the nanoparticle system, which is proportional to mean anisotropy barrier, i.e., $T_B \sim KV$, K being the anisotropy energy constant and V the mean nanoparticle volume. Since the volume is kept roughly constant within each series, the anomalous T_B for **Rha{Co_1Fe-6}**, which is lower than that of **Rha{$Co_{0.4}$Fe-6}**, might suggest a non-monotonous behavior of K in the 6 nm series.

The FC/ZFC curves of **Rha{$Co_{0.3}$Fe-6}** and **Rha{Co_1Fe-6}** present a jump around room temperature, due to the sudden activation of the Brownian motion at the water defreezing point that favors the alignment of the particle moments. This process, mainly relevant if T_B is close to the defreezing temperature, has been inhibited for **Rha{$Co_{0.4}$Fe-6}**, which has been measured as dried pellet, in order to clearly observe the ZFC maximum. The **Rha{Co_1Fe-10}** sample does not present a maximum in the ZFC curve (data not shown) suggesting that this sample, unlike the others, is not in the superparamagnetic regime in the experimental range of temperature (up to 350 K).

The magnetization as a function of the applied magnetic field was measured at 2.5 K in frozen solution and presented in Figures 4(B) (4 nm series) and (D) (6 nm series). All samples exhibit a hysteretic behavior that indicates that they are blocked at this temperature, as expected, but samples containing Co show a much larger coercivity. The coercive field $\mu_0 H_C$, indeed, suddenly increases from 0.004 T for $x = 0$ (magnetite) to 1.5–2.1 T for $x \neq 0$

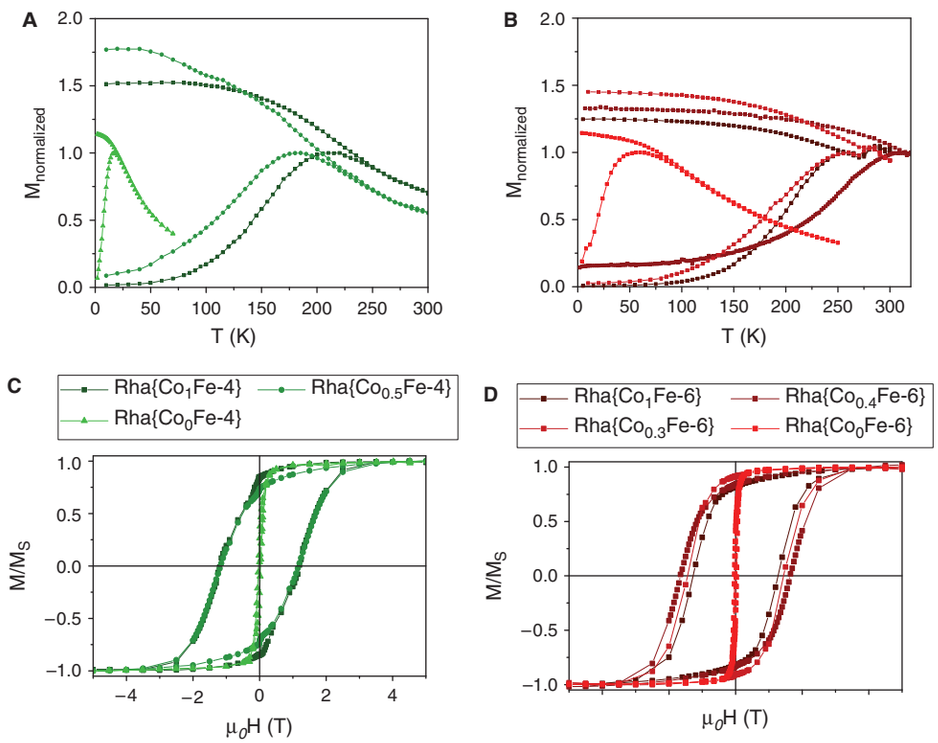

Figure 4. Experimental data from DC magnetic measurements of Rha{$Co_xFe_{3-x}O_4$} nanoparticles. ZFC/FC curves performed in solution for series with mean diameter ca. 4 nm (A) and 6 nm (B). Hysteresis loops for the series of $Co_xFe_{3-x}O_4$ nanoparticles of 4 nm (C) and 6 nm (D) performed in frozen solution at 2.5 K.

(cobalt ferrite). For stoichiometric cobalt ferrite nanoparticles ($x = 1$) the value of $\mu_0 H_C$ increase with the size of nanoparticles from 1.53 to 1.86 T. It is interesting to note that for 6 nm series $\mu_0 H_C$ value is not maximal for the stoichiometric structures but for intermediate doping levels ($x = 0.4$). We remind that the same trend with Co content is observed for T_B (T_{max}). Since both quantities $\mu_0 H_C$ and T_B strongly depend on the effective anisotropy of the nanosystem, we evaluated K, from the low temperature $\mu_0 H_C$ using relationship, $H_C = 0.96(K/M_S)[1 - (T/T_B)]^{0.77}$, where M_S is the saturation magnetization.[25, 26] All magnetic data in DC mode are reported in Table I. For magnetite nanoparticles, K values ca. 2×10^4 J·m^{-3} are obtained, in agreement with the corresponding bulk value (1.3×10^4 J·m^{-3}).[27] For cobalt ferrite nanoparticles, K values are in the range $(4.9–9.5) \times 10^5$ J·m^{-3}, which is higher than that of the bulk material (2×10^5 J·m^{-3}),[27] but consistent with the values observed for nanoparticles.[11, 25, 26, 28] As supposed, the K values show a trend similar to those of $\mu_0 H_C$ and T_B. Such a non-monotonous trend of K with Co doping level is coherent with previous results obtained by some of us on samples of Co-doped magnetite of 5 nm.[25]

For samples with cobalt ions ($x > 0$), an increase of the reduced remnant magnetization, M_R/M_S, is observed up to 0.7–0.9. These values are typically observed in the case of cubic anisotropy, for which M_R/M_S value is theoretically foreseen equal to 0.83.[29] It is important to note that a stoichiometric structure of cobalt ferrite ($x = 1$) is not needed to observe a cubic anisotropy.

In order to investigate the relaxation dynamics of these samples, the temperature dependence of the in-phase (χ') and the out-of-phase (χ'') components of the magnetic susceptibility were measured in AC mode for eight frequencies, f, logarithmic spaced in the 0.1–1000 Hz range. Samples **Rha{Co$_{0.4}$Fe-6}** and **Rha{Co$_1$Fe-10}** were not measured as their T_{max} is higher than 300 K. As typical example, the AC susceptibility curves for **Rha{Co$_0$Fe-6}** and **Rha{Co$_1$Fe-4}** samples are shown in Figures 5(A) and (B), respectively.

As a first approximation, the frequency dependence of the ac susceptibility was fitted according to the Néel model, which relates the blocking temperature with the observation time, τ, as: $\tau = \tau_0 \exp(E_a/k_B T_B)$, where $E_a = KV$ is the energy barrier and τ_0 the attempt time. The linear curves of Figures 5(C) and (D) are obtained by plotting the observation times $\tau = 1/2\pi f$ versus the inverse of the blocking temperatures obtained from the χ'' maxima recorded for different frequencies. The best fit parameters E_a and τ_0 values are listed in Table II. For magnetite samples ($x = 0$), τ_0 is in the 10^{-9}–10^{-12} s^{-1} range, indicating a pure superparamagnetic behavior of isolated nanoparticles. For Co^{2+} doped samples, a dramatic decrease of τ_0 was observed. According to the most common explanation, this feature can be associated to the

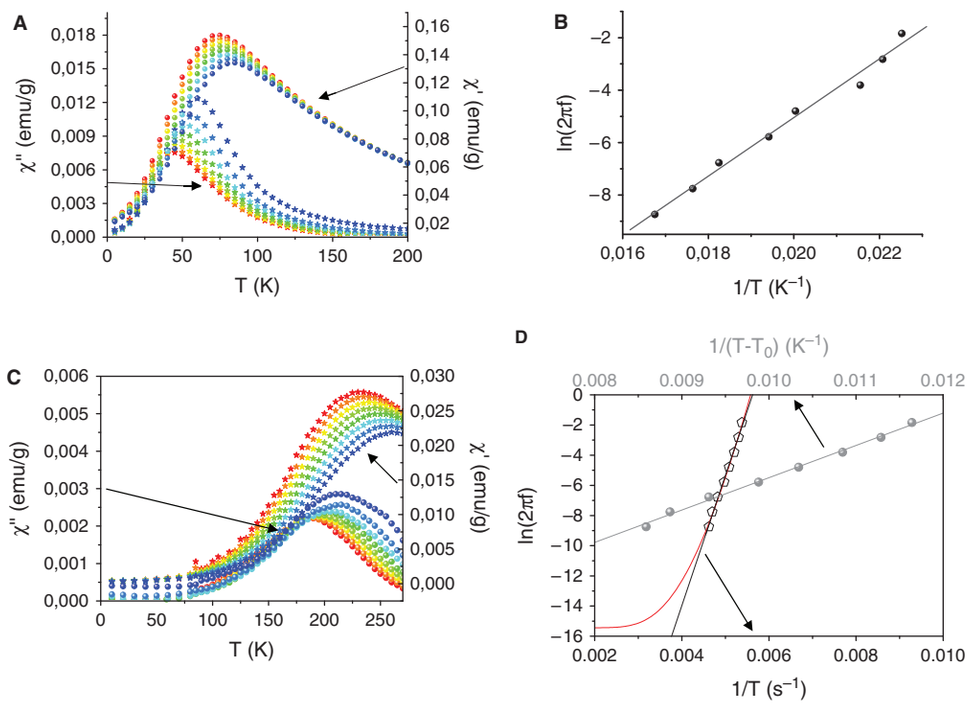

Figure 5. AC measurements for two samples of Rha{$Co_xFe_{3-x}O_4$} nanoparticles. In phase, χ', and out-phase, χ'', components of AC susceptibility measurement for (A) Rha{Co_0Fe-6}, and (C) Rha{Co_1Fe-4} samples performed with 8 logarithmic spaced frequencies from 0.1 to 1000 kHz. Linear plot of $\ln(2\pi f)$ versus $1/T_{max}$ for (B) Rha{Co_0Fe-6} and (D) Rha{Co_1Fe-4} samples according to the Néel (dark), the Vogel-Fulcher (grey) and Torres et al. (red) model.

Table II. Magnetic data obtained applying Arrhenius and Vogels-Fulcher models to AC measurement data. τ_0, attempt time (values in the 10^{-9}–10^{-12} s range are foreseen for non-interacting nanoparticles in a pure superparamagnetic regime); E_a/k_B, energy barrier; T_0 temperature of a spin-glass-like transition and B, parameter to account for K_{eff} temperature dependence, as reported in work of Torres et al.[31]

	Arrhenius plot		Vogel-Fulcher plot			Torres model		
	τ_0 (s)	E_a/k_B (K)	τ_0 (s)	E_a/k_B (K)	T_0 (K)	τ_0 (s)	E_a/k_B (K)	B (K^{-2})
Rha{Co_0Fe-4}	1.1×10^{-12}	337	/	/	/	/	/	/
Rha{$Co_{0.5}$Fe-4}	8.6×10^{-19}	6336	1.88×10^{-12}	2242	71	1.7×10^{-6}	8600	6×10^{-5}
Rha{Co_1Fe-4}	9.6×10^{-22}	8600	2.05×10^{-12}	2142	100	2.5×10^{-7}	10 600	4×10^{-5}
Rha{Co_0Fe-6}	1.3×10^{-12}	1325	/	/	/	/	/	/
Rha{$Co_{0.3}$Fe-6}	6.0×10^{-39}	20141	1.50×10^{-12}	1384	180	7.5×10^{-7}	171 300	7×10^{-5}
Rha{$Co_{0.4}$Fe-6}	/	/	/	/	/	/	/	/
Rha{Co_1Fe-6}	5.2×10^{-32}	19461	1.56×10^{-12}	2034	198	5×10^{-6}	207 400	6×10^{-5}
Rha{Co_1Fe-10}	/	/	/	/	/	/	/	/

presence of dipolar interaction among the nanoparticles. To test this assumption, the experimental data were fitted with the Vogel-Fulcher law (VF),[30] which includes an additional parameter, i.e., a spin-glass-like transition temperature T_0, to account for interactions (Table II). The VF results for Co doped samples show τ_0 in the 10^{-9}–10^{-12} s^{-1} range, and relatively high T_0 values which are indicative of strong dipolar interactions, although measurements have been performed in solution. Since dipolar interaction essentially depends on the magnetic moment of the single nanoparticles and on the distance among them, this result implies that Co doped nanoparticles are closer each other's than magnetite ones, being the magnetic moment of the latter higher than that of the first ones. As the presence of a larger number of aggregates in the Co doped samples cannot be proved experimentally and cannot easily justified, we also considered a different approach to explain the unphysical values of τ_0, based on the model suggest by Torres et al.,[31] who proposed to fit the experimental data to the Arrhenuis law where the anisotropy constant K depends on the temperature. In this case, an additional parameter, B, is introduced, to account for the temperature dependence of K. Despite the assumptions of this model seem more reasonable in our case, the τ_0 values are not completely satisfying, as they are more than two orders of magnitude higher than the expectations (Table II). Moreover, the values of the energy barrier and thus of the effective anisotropy constant, $K_{\text{eff}} = E_a/V$, are extremely high and, contrary to the expectations, tend to increase for larger particles ($K_{eff} \approx 1 - 3 \times 10^7$ J/m^3 for **Rha{$Co_{0.6}$Fe-6}** and **Rha{Co_1Fe-6}**, respectively). We must remark, however, that the difficulties in finding a satisfying model derives both from our systems, which, due to the high nanoparticle concentration, cannot be considered as merely non-interacting, and from the limited frequency range we can explore to provide experimental data to test the proposed fitting laws.

3.3. Heating Capabilities

Calorimetric measurements were carried out under an alternating magnetic field of amplitude $H = 21$ kA/m and frequency $f = 168$ kHz. The SAR values obtained for the investigated series of cobalt ferrite nanoparticles are presented in Table I. In comparison with magnetite nanoparticles ($x = 0$) for which no temperature rise is observed, a heat generation is recorded even for small sizes of cobalt ferrite nanoparticles. Indeed, SAR values are 6 $W \cdot g^{-1}$ and 21 $W \cdot g^{-1}$ for **Rha{$Co_{0.5}$Fe-4}** and **Rha{Co_1Fe-4}**, respectively. SAR values do not follow a linear evolution with Co content. Indeed 2, 44, 22 and 32 W/g are observed for 6 nm series for $x = 0$, 0.3, 0.4 and 1, respectively. This trend may be correlated with the evolution observed for the anisotropy constant (Table I), which is higher for intermediated values of x. However, SAR of **Rha{$Co_{0.4}$Fe-6}** is less than the sample where $x = 0.3$ although its anisotropy constant is higher. This fact can be partially explained by smaller size and the higher polydispersity of **Rha{$Co_{0.4}$Fe-6}** compared to **Rha{$Co_{0.3}$Fe-6}**. For stoichiometric cobalt ferrite nanoparticles, an increase of the SAR values with size, from 21 $W \cdot g^{-1}$ for **Rha{Co_1Fe-4}** to 232 $W \cdot g^{-1}$ for **Rha{Co_1Fe-10}** is observed. The SAR value of 232 $W \cdot g^{-1}$ obtained for **Rha{Co_1Fe-10}** with a frequency/field of 168 kHz/21 kA/m shows undoubtedly the best heat capacity of the all the investigated samples.

4. CONCLUSION

In this work, we designed water dispersible rhamnose-functionalized cobalt ferrite $Co_xFe_{3-x}O_4$ nanoparticles of different size (from 4 to 10 nm) having different Co^{2+} content ($x = 0 - 1$) by using a three steps approach and adapting the experimental conditions. The solubility of these nanoparticles in water is possible thanks to the rhamnose derivative functionalization through the phosphonate anchoring functions; the latter covalently attached the rhamnose moiety to the nanoparticles surface. The nanoparticles present a high crystallinity (diameters estimated by TEM and XRD are similar), a narrow size distribution and they keep their cobalt ferrite structure after rhamnose grafting. The investigation of the magnetic properties indicates that the doping of ferrite spinel structure with Co^{2+} ions induces an important increase of magnetocrystalline anisotropy by a factor of about 30 compared

to analogue magnetite nanoparticles of similar size. However, as previously reported, the maximum increase of the anisotropy constant K is not achieved for stoichiometric cobalt ($x = 1$), but for intermediate level of cobalt doping. Samples with $x \neq 0$ present strong dipolar interactions even if the nanoparticles are dispersed in solution. Finally, an increase in Co^{2+} contain and/or in size leads to improve the magneto-thermal properties of the nanoparticles. Sample **Rha{Co_1Fe-10}** shows the best heating properties with a SAR of 232 W/g under an alternating magnetic field of $f = 168$ kHz and $H = 21$ kA $\cdot$ m^{-1}. The obtained results show that cobalt ferrite nanoparticles present an important potential as hyperthermia agents.

Acknowledgments: The authors thank Dr. G. Baldi and Dr. C. Ravagli from Ce.Ri.Col-Colorobbia Italia, C. Rebeil (PAC ICGM, University of Montpellier, France) for assistance for calorimetric and magnetic measurements. Claudia Innocenti and C. S. gratefully acknowledge the financial support of EC through COST Action RADIOMAG (TD1402). Joulia Larionova, Lenaic Lartigue, Yannick Guari thank the University of Montpellier and CNRS for financial support. Lenaic Lartigue thanks the UFI (GF/IR/732/07, n°25) for financial support.

References and Notes

1. A. K. Gupta and M. Gupta, *Biomaterials* 26, 3995 (**2005**).
2. A. Virden, S. Wells, and K. O'Grady, *J. Magn. Magn. Mater.* 316, 768 (**2007**).
3. M. A. Dobrovolskaia, S. E. McNeil, and S. E. M. Neil, *Nat. Nanotechnol.* 2, 469 (**2007**).
4. D. S. Kohane and R. Langer, *Chem. Sci.* 1, 441 (**2010**).
5. D. F. Williams, *Biomaterials* 29, 2941 (**2008**).
6. J.-P. Fortin, C. Wilhelm, J. Servais, C. Ménager, J.-C. Bacri, and F. Gazeau, *J. Am. Chem. Soc.* 129, 2628 (**2007**).
7. Y. II Kim, D. Kim, and C. S. Lee, *Phys. B Condens. Matter.* 337, 42 (**2003**).
8. T. Pannaparayil and S. Komarneni, *IEEE Trans. Magn.* 25, 4233 (**1989**).
9. N. Moumen and M. P. Pileni, *Chem. Mater.* 8, 1128 (**1996**).
10. Y. Li and C.-W. Park, *Langmuir* 15, 952 (**1999**).
11. S. Laureti, G. Varvaro, A. M. Testa, D. Fiorani, E. Agostinelli, G. Piccaluga, A. Musinu, A. Ardu, and D. Peddis, *Nanotechnology* 21, 15701 (**2010**).
12. F. Fiévet, S. Ammar-Merah, R. Brayner, F. Chau, M. Giraud, F. Mammeri, J. Peron, J.-Y. Piquemal, L. Sicard, and G. Viau, *Chem. Soc. Rev.* 47, 5187 (**2018**).
13. G. Baldi, D. Bonacchi, C. Innocenti, G. Lorenzi, and C. Sangregorio, *J. Magn. Magn. Mater.* 311, 10 (**2007**).
14. R. Topkaya, Ö. Akman, S. Kazan, B. Aktaş, Z. Durmus, and A. Baykal, *J. Nanoparticle Res.* 14, 1156 (**2012**).
15. Z. Beji, L. S. Smiri, N. Yaacoub, J.-M. Grenche, N. Menguy, S. Ammar, and F. Fiévet, *Chem. Mater.* 22, 1350 (**2010**).
16. H. Yang, C. Zhang, X. Shi, H. Hu, X. Du, Y. Fang, Y. Ma, H. Wu, and S. Yang, *Biomaterials* 31, 3667 (**2010**).
17. S. Sun, H. Zeng, D. B. Robinson, S. Raoux, P. M. Rice, S. X. Wang, and G. Li, *J. Am. Chem. Soc.* 126, 273 (**2004**).
18. E. Alphandéry, S. Faure, O. Seksek, F. Guyot, and I. Chebbi, *J. Phys. Chem. C* 115, 11920 (**2011**).
19. L. Lartigue, C. Innocenti, T. Kalaivani, A. Awwad, M. del M. Sanchez Duque, Y. Guari, J. Larionova, C. Guérin, J.-L. G. Montero, V. Barragan-Montero, P. Arosio, A. Lascialfari, D. Gatteschi, and C. Sangregorio, *J. Am. Chem. Soc.* 133, 10459 (**2011**).
20. B. Kang, T. Opatz, K. Landfester, and F. R. Wurm, *Chem. Soc. Rev.* 44, 8301 (**2015**).
21. N. C. Reichardt, M. Martín-Lomas, and S. Penadés, *Chem. Soc. Rev.* 42, 4358 (**2013**).
22. V. Barragan-Montero, J.-Y. Winum, J.-P. Molès, E. Juan, C. Clavel, and J.-L. Montero, *Eur. J. Med. Chem.* 40, 1022 (**2005**).
23. Y. Hou, Z. Xu, and S. Sun, *Angew. Chem. Int. Ed.* 46, 6329 (**2007**).
24. L. Lartigue, K. Oumzil, Y. Guari, J. Larionova, C. Guérin, J.-L. Montero, V. Barragan-Montero, C. Sangregorio, A. Caneschi, C. Innocenti, T. Kalaivani, P. Arosio, and A. Lascialfari, *Org. Lett.* 11, 2992 (**2009**).
25. E. Fantechi, G. Campo, D. Carta, A. Corrias, C. de Julián Fernández, D. Gatteschi, C. Innocenti, F. Pineider, F. Rugi, and C. Sangregorio, *J. Phys. Chem. C* 116, 8261 (**2012**).
26. E. Fantechi, C. Innocenti, M. Albino, E. Lottini, and C. Sangregorio *J. Magn. Magn. Mater.* 380, 365 (**2015**).
27. E. P. Wohlfarth, A Handbook on the Properties of Magnetically Ordered Substances, Elsevier (**1980**).
28. D. Peddis, F. Orrù, A. Ardu, C. Cannas, A. Musinu, and G. Piccaluga, *Chem. Mater.* 24, 1062 (**2012**).
29. M. Walker, P. I. Mayo, K. O'Grady, S. W. Charles and R. W. Chantrell, *J. Phys. Condens. Matter.* 5, 2779 (**1993**).
30. S. Shtrikman and E. P. Wohlfarth, *Phys. Lett.* 85, 467 (**1981**).
31. T. E. Torres, E. Lima Jr., A. Mayoral, A. Ibarra, C. Marquina, M. R. Ibarra, and G. F. Goya, *J. Appl. Phys.* 118, 183902 (**2015**).

Received: 5 July 2018. Accepted: 14 November 2018.